

TWO DISCRETE MEMRISTIVE CHAOTIC MAPS AND ITS DSP IMPLEMENTATION

XINTONG HAN ,*,† JUN MOU ,*,†,§,|| JINSHI LU ,*,¶,||
SANTO BANERJEE  and YINGHONG CAO ,†

**School of Mechanical Engineering and Automation
Dalian Polytechnic University
Dalian 116034, P. R. China*

†*School of Information Science and Engineering
Dalian Polytechnic University
Dalian 116034, P. R. China*

‡*Department of Mathematical Sciences
Giuseppe Luigi Lagrange, Politecnico di Torino
Corso Duca degli Abruzzi 24, Torino, Italy*

moujun@csu.edu.cn
lujs@dlpu.edu.cn

Received June 14, 2022

Accepted December 1, 2022

Published May 4, 2023

||Corresponding authors.

This is an Open Access article in the “Special Issue on Artificial Intelligence, Machine Learning and Big Data Applications for Chaotic and Nonlinear Modelling in Social Sciences, Economics and Finances”, edited by Hadi Jahanshahi (Institute of Electrical and Electronics Engineers, Canada) & Stelios Bekiros (University of Malta, Malta) & London School of Economics and Political Science, UK & IPAG Business School, France), published by World Scientific Publishing Company. It is distributed under the terms of the Creative Commons Attribution 4.0 (CC BY) License which permits use, distribution and reproduction in any medium, provided the original work is properly cited.

Abstract

In this paper, a discrete model of memristor is adopted and analyzed. The new discrete maps are built by introducing this discrete memristor model into a two-dimensional discrete map. Interestingly, introducing this discrete memristor model from different locations can lead to two new chaotic map models. The dynamical behaviors of the two maps are studied by means of bifurcation diagrams, phase diagrams and Lyapunov exponential spectra (LEs). The simulation results show that both chaotic systems have rich dynamical behaviors. In addition, they are experimentally found to have multi-stable properties, where the M-XM map has infinite attractors coexistence. Finally, we complete the hardware implementation of the two maps based on Digital Signal Processing (DSP) platform for the application of discrete chaotic systems.

Keywords: Chaotic Map; Memristor Model; Infinite Attractors Coexistence; Hardware Implementation.

1. INTRODUCTION

In 1971, Professor Chua of the University of California, Berkeley, proposed the existence of a fourth passive fundamental circuit element.¹ Professor Chua named it memristor,² which is used to characterize the relationship between magnetic flux and charge. However, it did not receive widespread attention until 2008, when Hewlett-Packard's laboratory reported the achievability of the memristor.³ The appearance of this result set off a wave of scholarly research related to memristors. In recent years, the research on memristive had become more and more extensive, and has had an extremely important impact on many disciplines.^{4,5} Memristors are mainly used in various fields in the form of circuits,^{6,7} such as artificial intelligence computers,^{8–10} secure communications,^{11–13} artificial neural networks,^{14–16} and memristive chaotic oscillator circuits.^{17–19} However, most of the related research on memristor is continuous,²⁰ and the related research on discrete memristor deserves further exploration.

In practice, with the deepening of the research on memristors, some scholars had found that the characteristics of memristors can make the system appear more complex dynamical behaviors. Therefore, memristors have also been well used in the field of chaos.^{21–25} Chaos theory is an important part of nonlinear science and was first proposed in the early 19th century.^{26–28} Together with the theory of relativity and quantum mechanics, he is known as the three major scientific revolutions of the 20th century.^{29–31} The key to the research of chaos theory is to seek the internal order structure hidden in the unpredictable irregular phenomenon, which makes it possible for scholars to further explore the phenomenon that cannot be described, explained

or predicted by the existing paradigm.^{32–35} As an interesting and common form of motion, it is very necessary to explore and study chaos theory. Recently, discrete chaotic systems have attracted the research enthusiasm of many scholars. For example, Mikaeel *et al.*³⁶ studied the forecast of the system's behavior in future through the analytical solution and simulations. Yuan *et al.*³⁷ presented a method to generate chaos and hyperchaos by cascading discrete memristive maps. Based on the above, this paper discusses the dynamics of two discrete memristive systems by introducing a discrete memristive model into the discrete map.

The main frameworks of the following are set as follows. First, the mathematical models of the systems studied in this paper are given in the part of "System Model", and the balance points of the model are classified and discussed. Next is the "Dynamical Analyses" part, where the dynamical evolution and attractor coexistence of the two system models with parameter changes are given. In addition, the "Hardware Implementation" part completes the attractor phase diagram of the two models through the experiment platform of Digital Signal Processing (DSP). Finally, the conclusion section summarizes the findings of this paper.

2. SYSTEM MODEL

2.1. Three-Dimensional Memristor Map Construction

In the section, a discrete memristor model is adopted,³⁸ it can be expressed as

$$\begin{cases} v_n = M(q_n)i_n = (\alpha + \beta q_n^2)i_n, \\ q_{n+1} = q_n + \Delta T i_n, \end{cases} \quad (1)$$

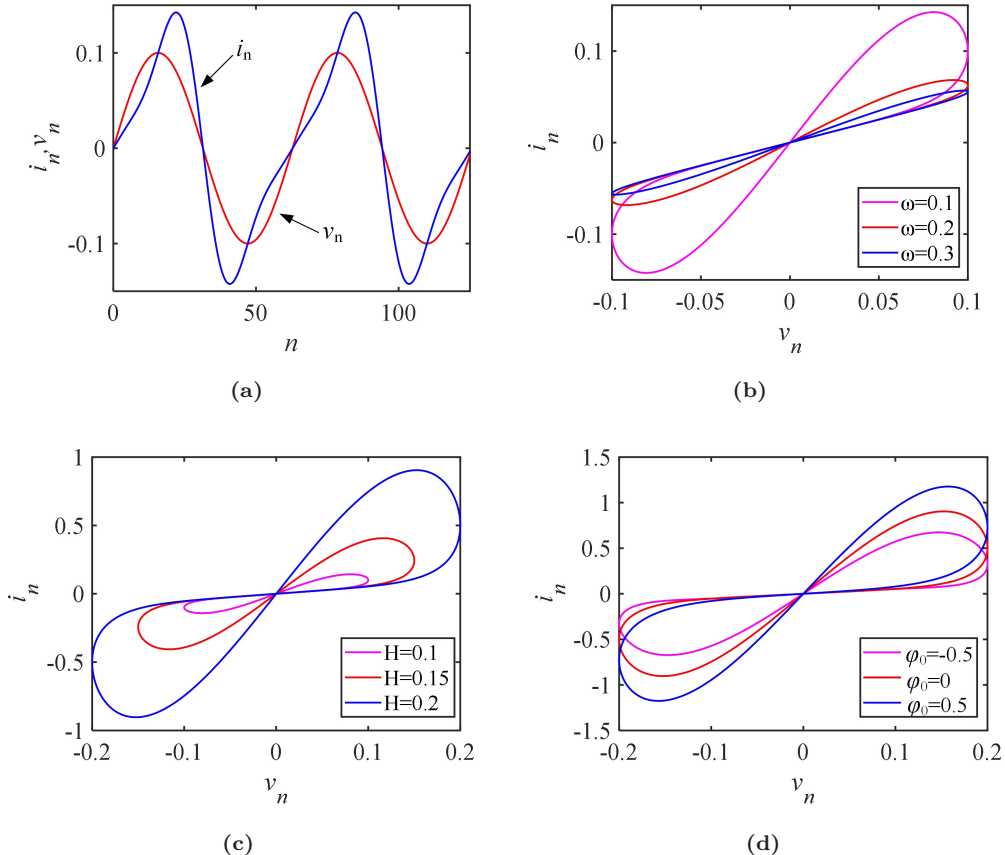


Fig. 1 Simulation results of the characteristics of the discrete model of memristor. (a) Inputs and outputs with the number of iterations; (b) $\phi_0 = 0$, $H = 0.1$; (c) $\omega = 0.1$, $\phi_0 = 0$; (d) $\omega = 0.1$, $H = 0.1$.

where ΔT denotes the step size (generally set to 1), q_n is an internal state variable. To observe the memristive features of this discrete memristor model, a discrete sinusoidal current i_n ($i_n = H \sin(\omega_n)$) is given to the discrete memristor model. Let $\alpha = 0.5$, $\beta = 0.5$, the characteristic curves of this discrete memristor model are plotted, as shown in Fig. 1. Among them, Fig. 1a shows inputs and outputs that vary with the number of iterations. Figures 1b–1d are the voltametric characteristic curves of the memristor under different parameters.

Zhang *et al.*³⁹ proposed a two-dimensional (2D) map with infinitely many coexisting attractors by introducing sinusoidal functions into a class of 2D maps. Its mathematical model can be expressed as

$$\begin{cases} x_{k+1} = x_k + ax_k \sin(y_k), \\ y_{k+1} = y_k + bx_k + c, \end{cases} \quad (2)$$

where $a \neq 0$, $b \neq 0$, and $c \neq 0$. Based on the above, assuming that the input of the discrete model of memristor is a variable, introducing it into the 2D discrete map, then a new three-dimensional chaotic

system can be obtained. Depending on the different positions introduced by the discrete memristor, we can obtain two different three-dimensional memristor maps (M-XM map and M-YM map).

M-XM map:

$$\begin{cases} x_{n+1} = x_n + ax_n \sin y_n + dx_n(\alpha + \beta z_n^2), \\ y_{n+1} = y_n + bx_n + c, \\ z_{n+1} = z_n + ex_n, \end{cases} \quad (3)$$

M-YM map:

$$\begin{cases} x_{n+1} = x_n + ax_n \sin y_n, \\ y_{n+1} = y_n + bx_n + c + dy_n(\alpha + \beta z_n^2), \\ z_{n+1} = z_n + ey_n. \end{cases} \quad (4)$$

2.2. Equilibrium Point Analysis

The equilibrium point analysis of chaotic systems is an important element in the qualitative analysis of chaotic mechanisms. Set the equilibrium point of the map be (x, y, z) , then the M-XM map can be

written as

$$\begin{cases} x = x + ax \sin y + dx(\alpha + \beta z^2), \\ y = y + bx + c, \\ z = z + ex. \end{cases} \quad (5)$$

Based on Eq. (5), the Jacobian matrix of the M-XM map can be obtained as follows:

$$J_1 = \begin{bmatrix} 1 + a \sin y + d(\alpha + \beta z^2) & ax \cos y & 2d\beta xz \\ b & 1 & 0 \\ e & 0 & 1 \end{bmatrix}. \quad (6)$$

In order to find the equilibrium point of the M-XM map, we will discuss it in two different cases.

Case A: $c = 0$.

At this point, the equilibrium point of the M-XM map is

$$E_1 = (0, k_1, k_2), \quad (7)$$

where k_1 and k_2 are arbitrary constants. It follows that the M-XM map has infinitely many fixed points in the plane. Bringing the equilibrium point E_1 into Eq. (6), one can get

$$J_1^* = \begin{bmatrix} 1 + a \sin k_1 + d(\alpha + \beta k_2^2) & 0 & 0 \\ b & 1 & 0 \\ e & 0 & 1 \end{bmatrix}, \quad (8)$$

$$\det(\lambda E - J_1^*) = 0. \quad (9)$$

At this point, the characteristic root is

$$\lambda_1 = \lambda_2 = 1, \quad \lambda_3 = 1 + a \sin k_1 + d(\alpha + \beta k_2^2). \quad (10)$$

The eigenvalues λ_1 and λ_2 are always located on the unit circle. The λ_3 determines the stability of the system. The system is stable when the system eigenvalues satisfy the following equation:

$$\lambda_3 = 1 + a \sin k_1 + d(\alpha + \beta k_2^2) \leq 1. \quad (11)$$

Case B: $c \neq 0$.

Bringing $c \neq 0$ into Eq. (5) shows that there is no fixed point in the M-XM map currently. Therefore, when $c \neq 0$, the attractors generated by the M-XM map are called the hidden attractors.

For the M-YM map, assume that the equilibrium point is (x^*, y^*, z^*) , we can obtain

$$\begin{cases} x^* = x^* + ax^* \sin y^*, \\ y^* = y^* + bx^* + c + dy^*(\alpha + \beta z^{*2}), \\ z^* = z^* + ey^*. \end{cases} \quad (12)$$

Then, the Jacobian matrix of the M-YM map is

$$J_2 = \begin{bmatrix} 1 + a \sin y & ax \cos y & 0 \\ b & 1 + d(\alpha + \beta z^2) & 2d\beta yz \\ 0 & e & 1 \end{bmatrix}. \quad (13)$$

Obviously, the solution of Eq. (12) is

$$E_2 = (0, 0, k), \quad (14)$$

where k is an arbitrary constant. So, the M-YM map has infinitely fixed points. Bringing Eq. (14) into Eq. (13), we can get the following:

$$J_2^* = \begin{bmatrix} 1 & 0 & 0 \\ b & 1 + d(\alpha + \beta k^2) & 0 \\ 0 & e & 1 \end{bmatrix}, \quad (15)$$

$$\det(\lambda E - J_2^*) = 0. \quad (16)$$

The characteristic root of the M-YM map is

$$\lambda_1 = \lambda_2 = 1, \quad \lambda_3 = 1 + d(\alpha + \beta k^2). \quad (17)$$

From the eigenroot discriminant, it is known that the system is stable when all eigenvalues are within the unit circle (including on the unit circle). Therefore, the fixed point of the system is stable when the following conditions are satisfied:

$$d(\alpha + \beta k^2) \leq 0. \quad (18)$$

3. DYNAMICAL ANALYSES

3.1. Dynamical Evolutions

In this section, the dynamical behaviors of the two map models with parameter variation are analyzed by computer simulation. In the following, we analyze the dynamical evolutions of the system mainly by bifurcation diagram and Lyapunov exponential spectrum with parameters a and b , respectively.

(1) The a varies

For the M-XM map, let the initial values be $[1, -3, 3]$, other parameters are set as $b = 1.3$, $c = 0.1$, $d = e = 0.005$, $\alpha = \beta = 0.5$. When $a \in (2.35, 2.73)$, the bifurcation figure and the corresponding Lyapunov exponential spectrum are

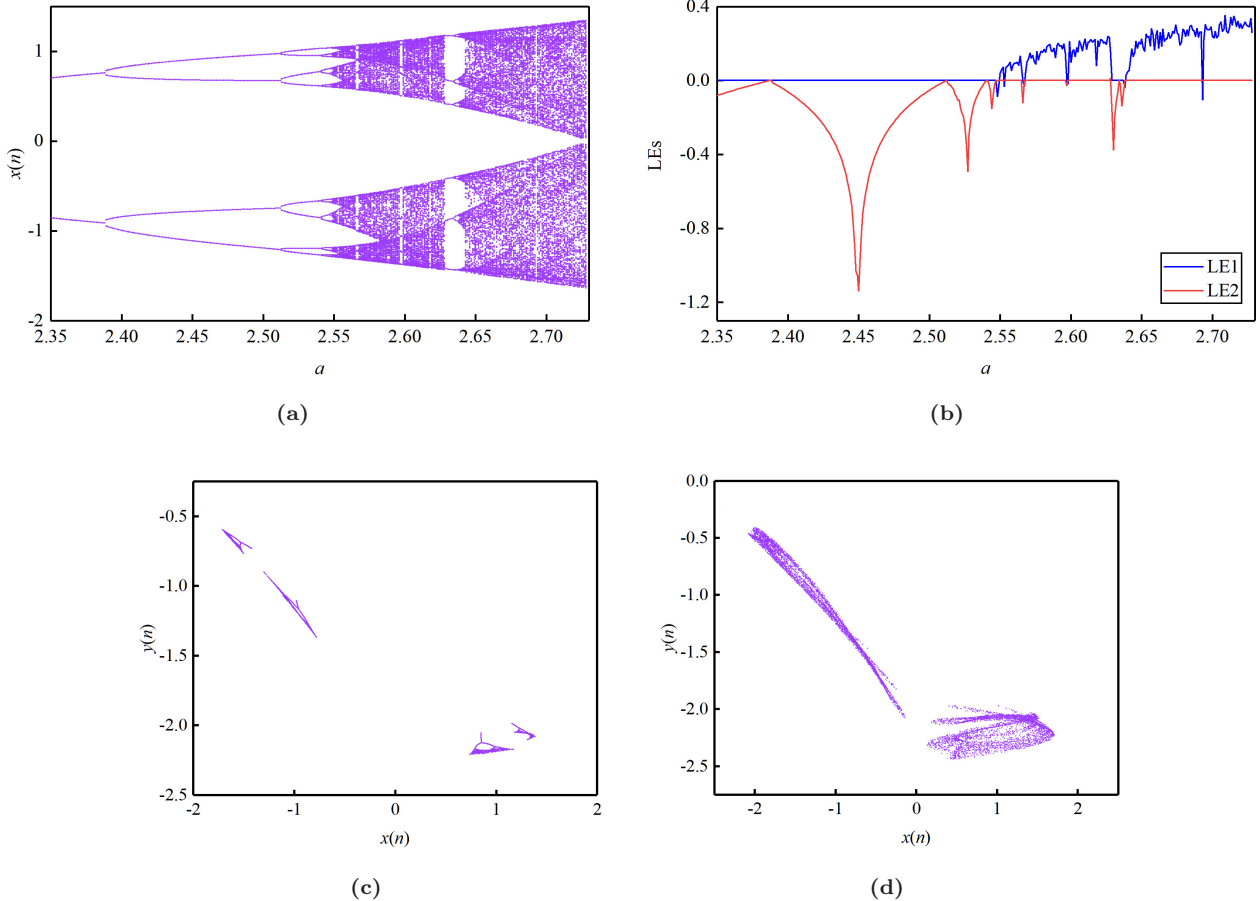


Fig. 2 Dynamical evolutions of the M-XM changes with the parameter a . **(a)** Bifurcation; **(b)** LEs; **(c)** $a = 2.575$; **(d)** $a = 2.72$.

shown in Figs. 2a and 2b. The multiplicative bifurcation behavior of the M-XM map can be clearly observed in Fig. 2a. When $a \in (2.35, 2.55) \cup (2.566, 2.568)$, the map is periodic. In the other ranges, the system is in chaotic state, which contains a window of three cycles. Two different types of singular attractors are plotted by taking $a = 2.575$ and $a = 2.72$, respectively.

For the M-YM map, set $b = 1.2$, $c = 0.1$, $d = 0.002$, $e = 0.001$, $\alpha = \beta = 0.1$, and $(x_0, y_0, z_0) = (1, -3, 7)$. When the parameter a changes from 2.33 to 2.73, the bifurcation of the M-YM map is shown as Fig. 3a, and Fig. 3b is corresponding diagram of Lyapunov exponential spectra (LEs). The bifurcation behavior of the map can be seen in the bifurcation diagram. The simulation results show that the Lyapunov exponential spectrum and bifurcation diagram the can be well corresponded. The map is chaotic when a belongs to $(2.571, 2.654)$ and $(2.664, 2.73)$. This includes four small cycle windows. Figures 3c and 3d are two phase diagrams of the M-YM map.

(2) The b varies

For the M-XM map, set $(x_0, y_0, z_0) = (1, -3, 2)$, $a = 2.7$, and other parameters remain unchanged. Figure 4a is the bifurcation diagram of the M-XM map when b varies from 0.345 to 1.48. As can be observed in Fig. 4, the map has a bifurcation behavior of multiplicative period. Figure 4b is the LEs of the M-XM map varies with the parameter b . When $b \in (0.5, 0.66) \cup (0.695, 1.255) \cup (1.27, 1.48)$, the map is chaotic state. The attractor phase diagrams obtained from the simulation are shown in Figs. 4c and 4d by taking two different sets of parameters, $b = 0.88$ and $b = 1.265$, respectively.

For the M-YM map, let $a = 2.68$, $c = 0.11$, other parameters are the same as above. The initial value $(x_0, y_0, z_0) = (1, -3, 5)$. The dynamical behavior of the system was analyzed when the parameter b was varied in the range of 0.2–1.65. The corresponding LEs and bifurcation diagram are shown in Figs. 5a and 5b. Figure 5b shows that the M-YM map is in the chaotic state throughout its range. It is interesting to see in Fig. 5a that the chaotic domain

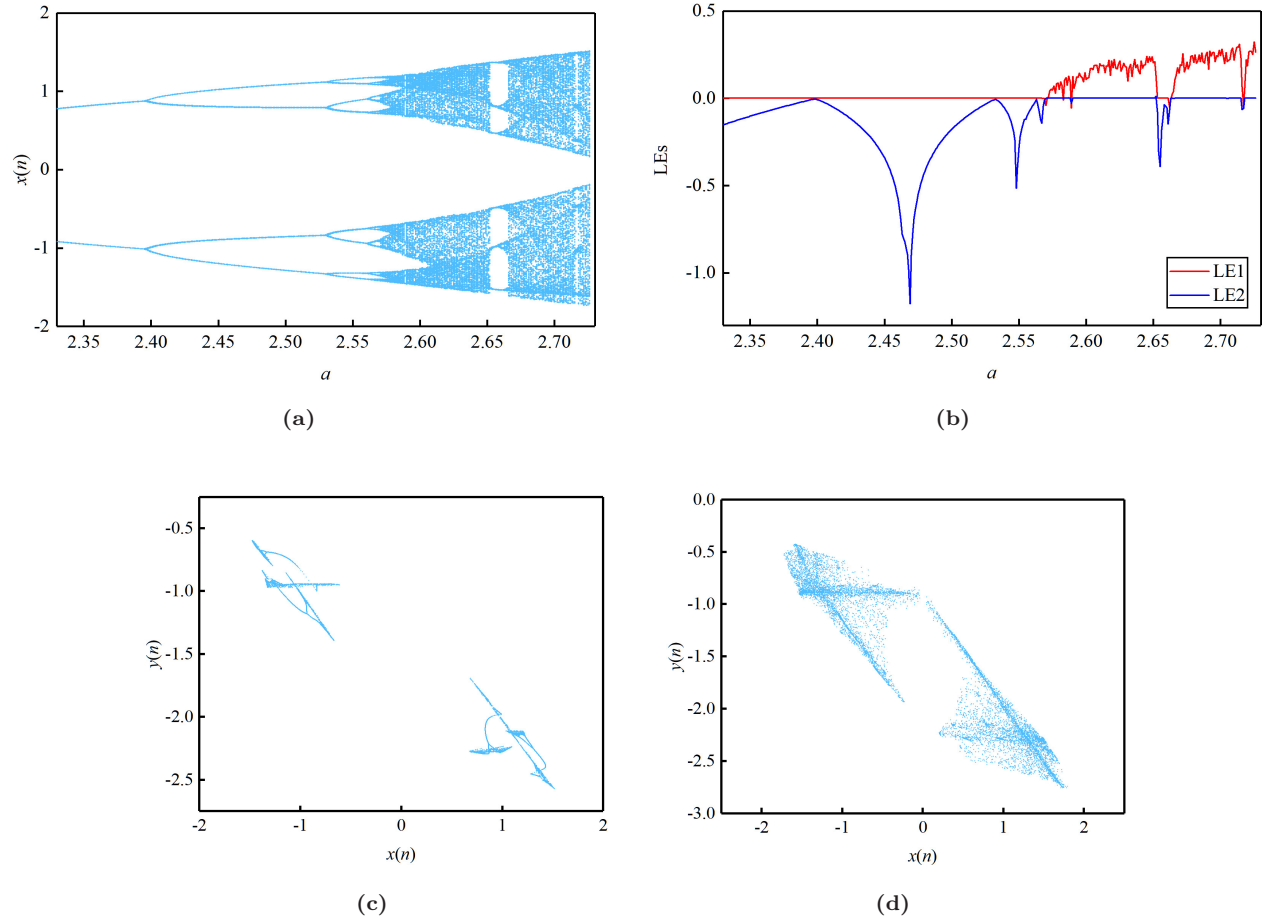


Fig. 3 Dynamical evolutions of the M-YM changes with the parameter a . **(a)** Bifurcation; **(b)** LEs; **(c)** $a = 2.6$; **(d)** $a = 2.72$.

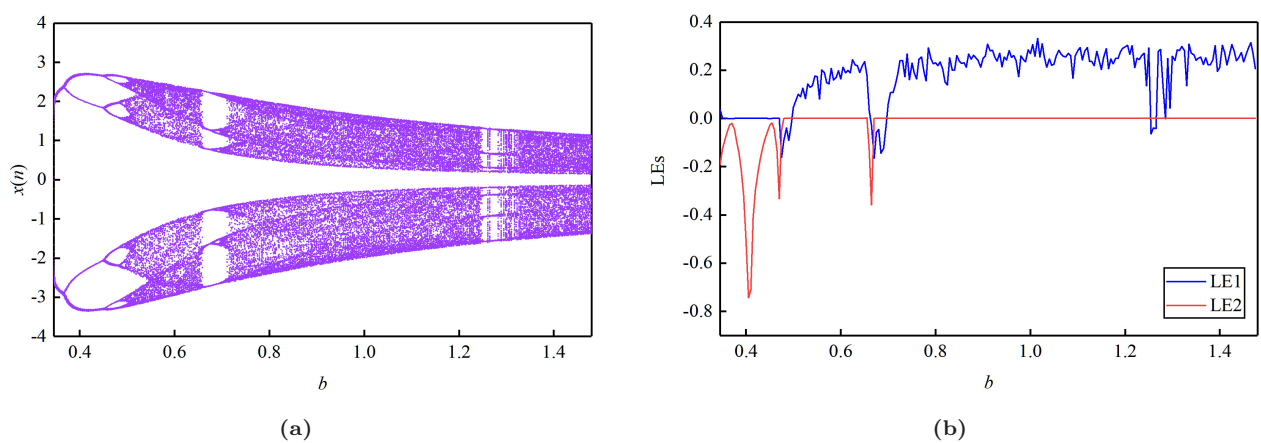


Fig. 4 Dynamical evolutions of the M-XM changes with the parameter b . **(a)** Bifurcation; **(b)** LEs; **(c)** $b = 0.88$; **(d)** $b = 1.265$.

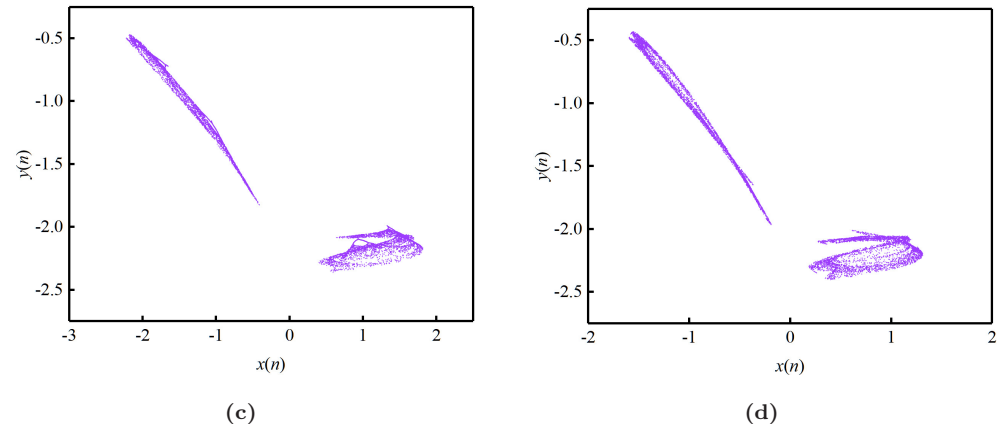
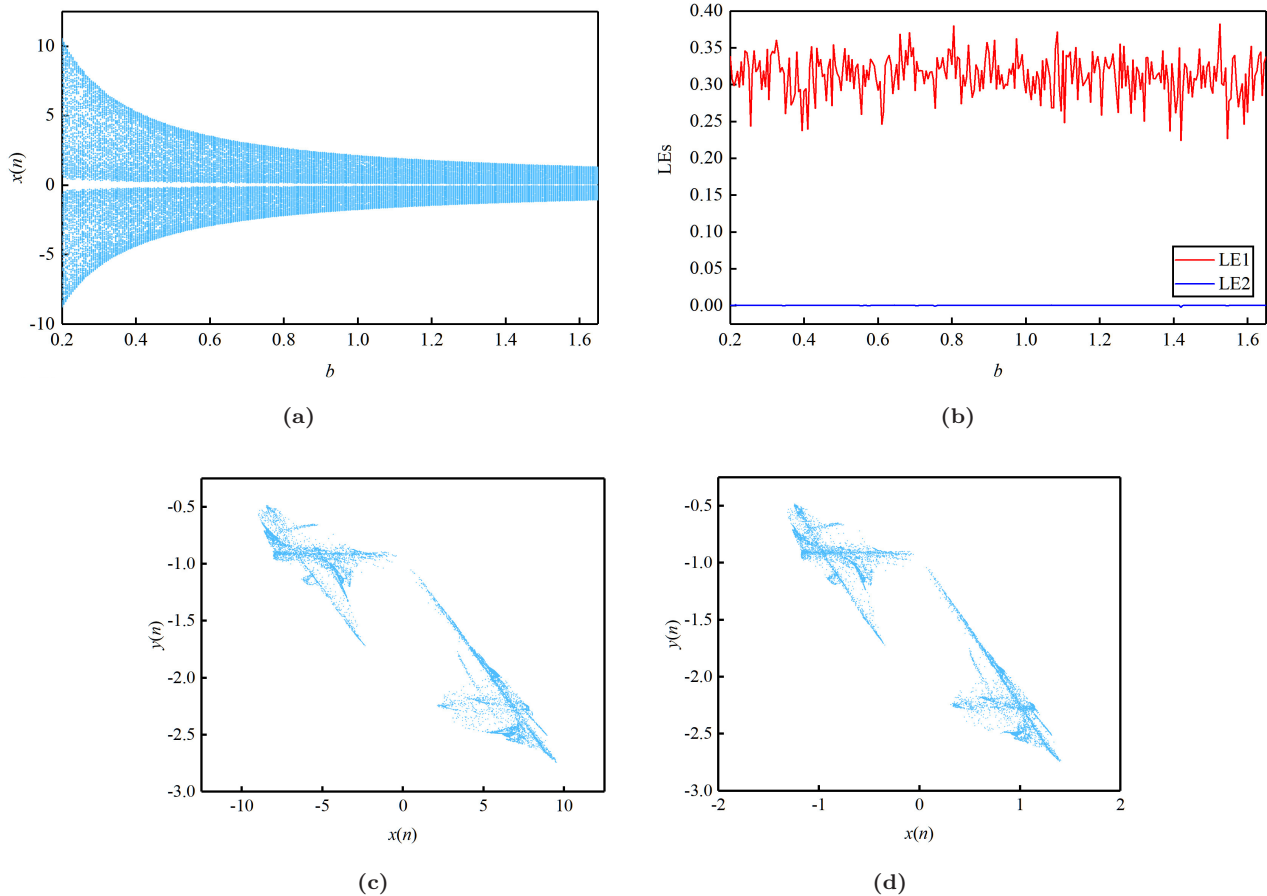


Fig. 4 (Continued)

Fig. 5 Dynamical evolutions of the M-YM changes with the parameter b . (a) Bifurcation; (b) LEs; (c) $b = 0.22$; (d) $b = 1.5$.

of the map decreases as the parameter b increases. On this point, the same conclusion can be drawn in Figs. 5c and 5d. Figures 5c and 5d show the phase diagrams of the M-YM map when b is taken as 0.22 and 1.5, respectively. They are similar in shape, but a closer look reveals that the lengths of their horizontal coordinates are different. The larger the value

of b , the smaller the range of their horizontal coordinates.

3.2. Coexisting Attractors

For a system, it is possible to obtain several different chaotic attractors when changing only the initial

value, and this phenomenon is called attractor coexistence. This phenomenon of the M-XM map and M-YM map is observed and analyzed in this part.

(1) The M-XM map

When analyzing the dynamical characteristics of the system with the initial value, we found the interesting phenomenon that the system has the coexistence of infinite attractors. When $a = 2.6$, $b = 0.7$, $c = 0.1$, the remaining parameters remain

unchanged, and the initial value $x_0 = 1$, $z_0 = 3$, the phase diagram for the phenomenon of attractors coexistence with different y_0 is plotted as Fig. 6a. The same shape of the attractors can be observed in the Fig. 6, but at different positions on the y -axis. As y_0 decreases, the positions of attractor move downward. Figure 7 is the diagram of coexisting attractors with different y_0 when $a = 2.7$, $b = 0.8$, $z_0 = 5$, and the remaining parameters and initial values remain unchanged.

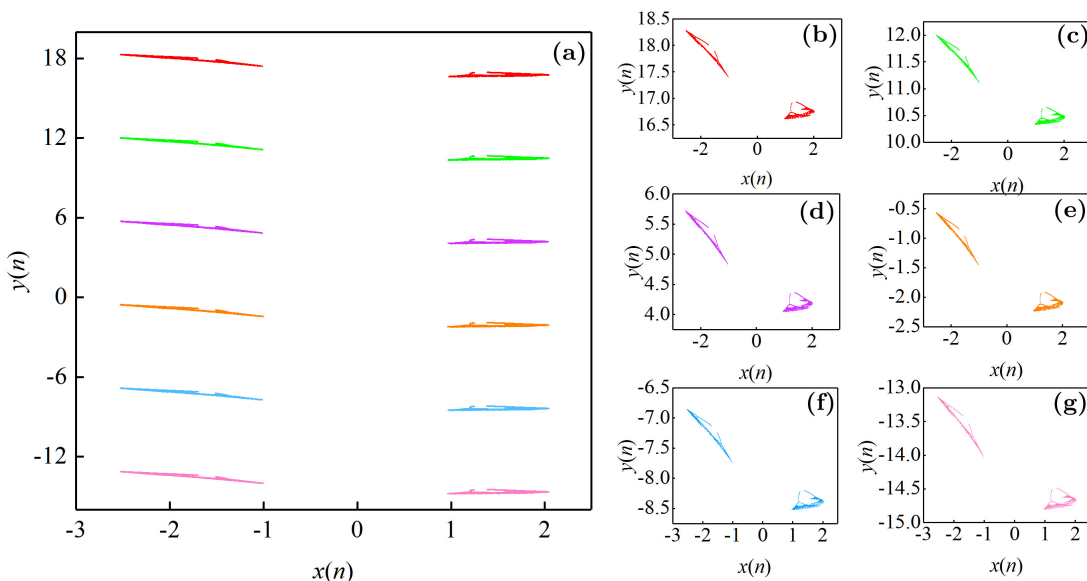


Fig. 6 Attractors phase diagrams. (a) Coexisting attractors; (b) $y_0 = 16$; (c) $y_0 = 10$; (d) $y_0 = 4$; (e) $y_0 = -2$; (f) $y_0 = -8$; (g) $y_0 = -15$.

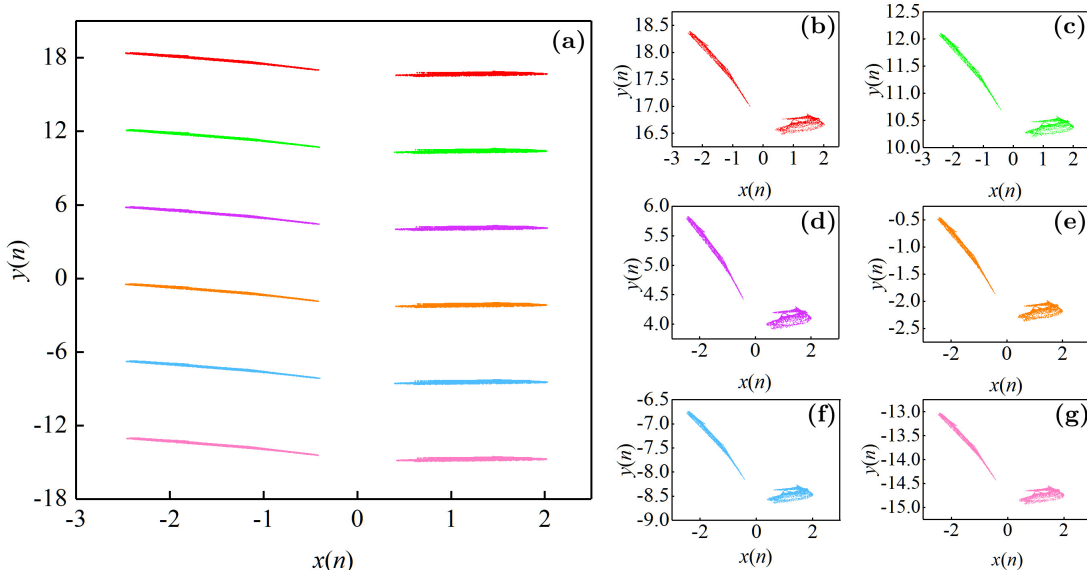


Fig. 7 Attractors phase diagrams. (a) Coexisting attractors; (b) $y_0 = 17$; (c) $y_0 = 10$; (d) $y_0 = 4$; (e) $y_0 = -2$; (f) $y_0 = -8$; (g) $y_0 = -14$.

(2) The M-YM map

Unlike the previous M-XM map, no infinite attractor coexistence was found in the analysis of the initial values of the M-YM map. In the experiment, it was found to have the coexistence of three different attractors. For further illustration, we take two sets of attractors phase diagrams with different

parameters as examples. Making $a = 2.65$, $b = 1$, $c = 0.1$, $d = 0.002$, $e = 0.001$, $\alpha = \beta = 0.1$, and other initial values $x_0 = 1$, $y_0 = -3$, the phase diagram of the three different attractors coexistence is shown in Fig. 8a. Among them, Figs. 8b–8d show the motion trajectories for different z_0 values, respectively. In addition, Fig. 9 is phase diagram of

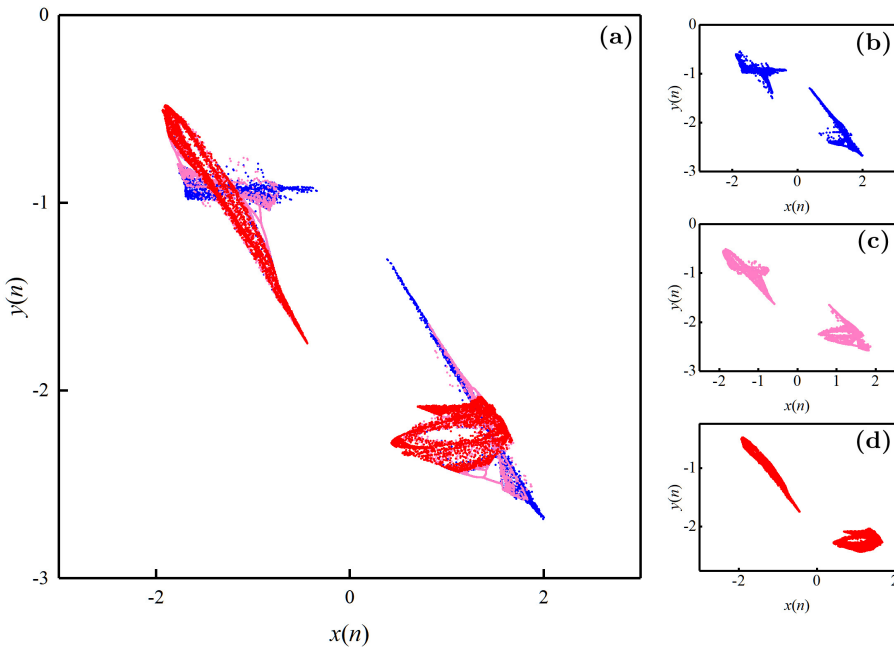


Fig. 8 Attractors phase diagrams. (a) Coexisting attractors; (b) $z_0 = -10$; (c) $z_0 = -6.6$; (d) $z_0 = 15$.

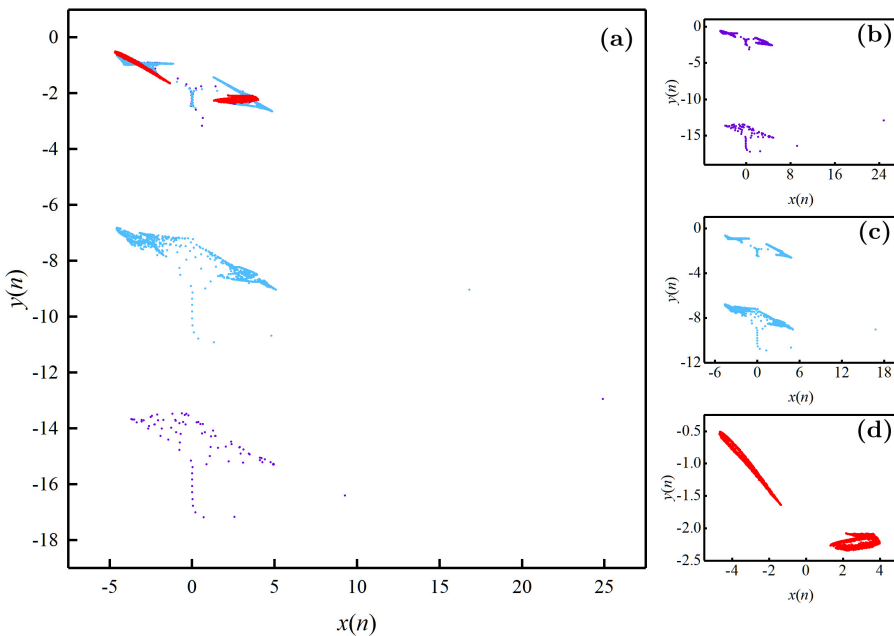


Fig. 9 Attractors phase diagrams. (a) Coexisting attractors; (b) $y_0 = -15$; (c) $y_0 = -7.5$; (d) $y_0 = -2.1$.

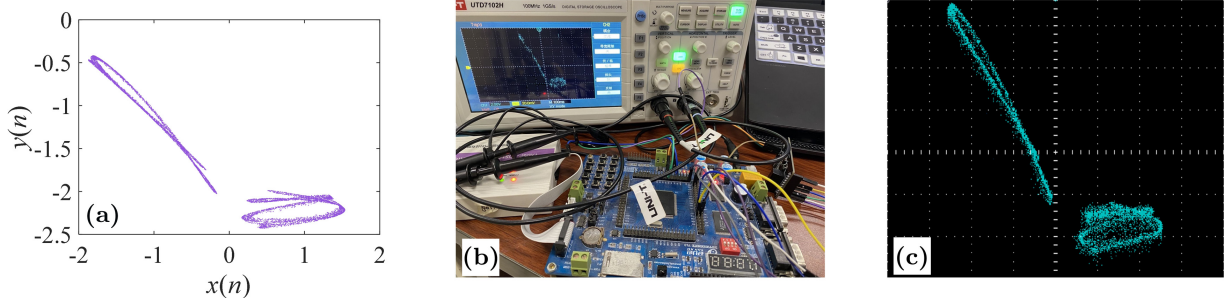


Fig. 10 Experimental diagram of the M-XM map. (a) computer simulation result; (b) experimental platform; (c) hardware implementation result.

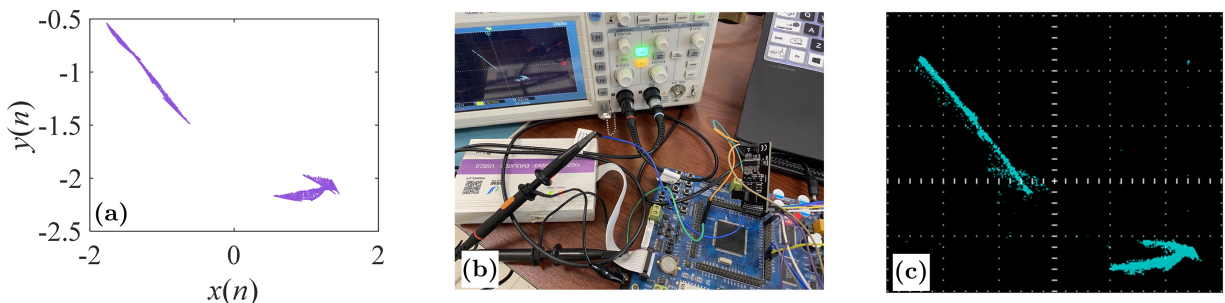


Fig. 11 Experimental diagram of the M-YM map. (a) computer simulation result; (b) experimental platform; (c) hardware implementation result.

the system when $a = 2.63$, $b = 0.4$, and the other parameters are intact. The initial values of Figs. 9b–9d are $(1, -15, 5)$, $(1, -7.5, 5)$, and $(1, -2.1, 5)$.

4. HARDWARE IMPLEMENTATION

Here, the two chaotic maps are implemented in hardware via the DSP platform. DSP chips, also called digital signal processors. DSP-based platform is chosen for digital circuit implementation because DSP has the advantages of large-scale integration, good stability, high accuracy, programmability, and easy interface. Figures 10b and 11b are pictures of the built experimental platform. The DSP chip (TMS320F28335), the communication interface (MAX3232), the DA converter (DAC8552), the oscilloscope, and the computer can be clearly seen in the pictures. For the M-XM map, let $a = 2.7$, $b = 1.1$, $c = 0.1$, $d = e = 0.005$, $\alpha = \beta = 0.5$, and the initial value is $(1, -3, 1)$. At this point, the phase diagram of the computer simulation and the result of the DSP achievement are shown in Figs. 10a and 10c. For the M-YM map, motion trajectory in phase space by computer simulation and corresponding DSP implementation results are displayed in Figs. 11a and 11c when $a = 2.56$, $b = 1$, $c = 0.14$,

$d = e = 0.001$, $\alpha = \beta = 0.1$, and (x_0, y_0, z_0) is $(-1, -1, 8)$. The experimental results show that the computer simulation results are very similar to the hardware implementation results, which can prove the feasibility of the two discrete systems in practical applications.

5. CONCLUSIONS

In the paper, the discrete model of memristor was chosen and its memristor characteristics were analyzed. Then, we introduced it into a 2D chaotic map. Since we introduce it from two different positions, two new chaotic maps are obtained, namely the M-XM map and the M-YM map. The analysis of the two systems from the perspective of equilibrium points shows that the two maps have infinitely many immobile points. Numerical simulations of the two systems are performed by computer to analyze their dynamical behaviors. The simulation results show rich dynamical behaviors of both systems. Interestingly, we found two systems with multi-stability, especially the M-XM map with infinite number of attractors coexisting. At last, we performed hardware implementation of the chaotic maps through the DSP platform. The hardware implementation

results are in high agreement with the computational and simulation results. The hardware implementation proves the feasibility of memristor map, and we will continue to explore the application of memristor map in the future.

ACKNOWLEDGMENTS

This work was supported by the Research on Electronic Component Assembly Robot (Grant No. 2022JJ12GX018); Research on Small Electronic Component Assembly Robot (Grant No. LJKZ0524).

ORCID

- X. Han  <https://orcid.org/0000-0003-2842-1803>
- J. Mou  <https://orcid.org/0000-0002-7774-2833>
- J. Lu  <https://orcid.org/0000-0002-9494-4146>
- S. Banerjee  <https://orcid.org/0000-0002-2135-695X>
- Y. Cao  <https://orcid.org/0000-0001-6154-8107>

REFERENCES

1. L. Chua, Memristor-The missing circuit element, *IEEE Trans. Circuit Theory* **18**(5) (1971) 507–519.
2. B. C. Bao, J. P. Xu and Z. Liu, Initial state dependent dynamical behaviors in a memristor based chaotic circuit, *Chin. Phys. Lett.* **27**(7) (2010) 51–53.
3. Y. Ho, G. M. Huang and P. Li, Dynamical properties and design analysis for nonvolatile memristor memories, *IEEE Trans. Circuits Syst. I: Regul. Pap.* **58**(4) (2011) 724–736.
4. J. Chen *et al.*, Multiply accumulate operations in memristor crossbar arrays for analog computing, *J. Semicond.* **42**(1) (2021) 90–111.
5. X. Wang *et al.*, A new four-dimensional chaotic system and its circuit implementation, *Front. Phys.* **10** (2022) 376.
6. B. Bao, Z. Liu and J. Xu, Transient chaos in smooth memristor oscillator, *Chin. Phys. B* **19**(3) (2010) 158–163.
7. L. Chua, If it's pinched it's a memristor, *Semicond. Sci. Technol.* **29**(10) (2014) 104001.
8. C. Mahata *et al.*, Controlled multilevel switching and artificial synapse characteristics in transparent HfAlO-alloy based memristor with embedded TaN nanoparticles, *J. Mater. Sci. Technol.* **95** (2021) 203–212.
9. S. Ke *et al.*, Brain-like synaptic memristor based on lithium-doped silicate for neuromorphic computing, *Front. Phys.* **17**(5) (2022) 53508.
10. K. Liao *et al.*, Memristor based on inorganic and organic two-dimensional materials: Mechanisms, performance, and synaptic applications, *ACS Appl. Mater. Interfaces* **13**(28) (2021) 32606–32623.
11. X. Li *et al.*, Design and DSP implementation of a fractional-order detuned laser hyperchaotic circuit with applications in image encryption, *Chaos Solitons Fractals* **159** (2022) 112133.
12. Y. Lin *et al.*, Nitrogen-induced ultralow power switching in flexible ZnO-based memristor for artificial synaptic learning, *Appl. Phys. Lett.* **118**(10) (2021) 103502.
13. Y. Sha *et al.*, A chaotic image encryption scheme based on genetic central dogma and KMP method, *Int. J. Bifurcation Chaos* **32**(12) (2022) 2250186.
14. H. Kim *et al.*, Neural synaptic weighting with a pulse-based memristor circuit, *IEEE Trans. Circuits Syst. I, Regul. Pap.* **59**(1) (2012) 148–158.
15. J. Shamsi *et al.*, Hardware implementation of differential oscillatory neural networks using VO₂-based oscillators and memristor-bridge circuits, *Front. Neurosci.* **15** (2021) 674567.
16. T. Ma *et al.*, A new class of Hopfield neural network with double memristive synapses and its DSP implementation, *Eur. Phys. J. Plus* **137** (2022) 4–19.
17. X. Wang *et al.*, Spintronic memristor through spin-torque-induced magnetization motion, *IEEE Electron Device Lett.* **30**(3) (2009) 294–297.
18. Z. Wang *et al.*, Memristors with diffusive dynamics as synaptic emulators for neuromorphic computing, *Nat. Mater.* **16**(1) (2017) 101–108.
19. W. Jiang *et al.*, Memristor-based multi-synaptic spiking neuron circuit for spiking neural network, *Chin. Phys. B* **31**(4) (2022) 40702–040702.
20. A. Akther *et al.*, Deterministic modeling of the diffusive memristor, *Chaos* **31**(7) (2021) 073111.
21. S. Wen *et al.*, CKFO: Convolution kernel first operated algorithm with applications in memristor-based convolutional neural network, *IEEE Trans. Comput.-Aided Des. Integr. Circuits Syst.* **40**(8) (2021) 1640–1647.
22. Y. Peng, S. He and K. Sun, Chaos in the discrete memristor-based system with fractional-order difference, *Results Phys.* **24** (2021) 104106.
23. M. Yildirim, DNA encoding for RGB image encryption with memristor based neuron model and chaos phenomenon, *Microelectron. J.* **104** (2020) 104878.
24. S. Kong *et al.*, A memristive map with coexisting chaos and hyperchaos, *Chin. Phys. B* **30**(11) (2021) 110502–110502.
25. X. Liu *et al.*, Memcapacitor-coupled Chebyshev hyperchaotic map, *Int. J. Bifurcation Chaos* **32**(12) (2022) 2250180.
26. N. G. Stephens *et al.*, Randomised controlled trial of vitamin E in patients with coronary disease:

- Cambridge heart antioxidant study (CHAOS), *Lancet* **347**(9004) (1996) 781–786.
27. M. M. Waldrop, Complexity: The emerging science at the edge of order and chaos, *Phys. Today* **45**(12) (1992) 83.
 28. X. Han *et al.*, A new set of hyperchaotic maps based on modulation and coupling, *Eur. Phys. J. Plus* **137** (2022) 523.
 29. O. E. Rössler, An equation for continuous chaos, *Phys. Lett. A* **57**(5) (1976) 397–398.
 30. X. L. Yu *et al.*, A novel method for radio frequency identification (RFID) multi-tag structure prediction based on a chaos algorithm and laser ranging, *Lasers Eng.* **48** (2021) 4–6.
 31. Q. J. Pan *et al.*, An efficient method combining polynomial-chaos kriging and adaptive radial-based importance sampling for reliability analysis, *Comput. Geotech.* **140** (2021) 104434.
 32. X. Zeng, L. Wan and H. Liu, Comparative analysis of three distribution entropy methods for chaos recognition, *J. Phys., Conf. Ser.* **1732** (2021) 012060.
 33. M. R. Tur and H. Ogras, Transmission of frequency balance instructions and secure data sharing based on chaos encryption in smart grid-based energy systems applications, *IEEE Access* **9** (2021) 27323–27332.
 34. N. An, Bringing order from the chaos of names, texts and nature: Collection and translation of Chinese *materia medica* in nineteenth-century Britain, *Front. Hist. China* **15**(1) (2020) 34–65.
 35. M. Abdelmalak and M. Benidris, A polynomial chaos-based approach to quantify uncertainties of correlated renewable energy sources in voltage regulation, *IEEE Trans. Ind. Appl.* **57**(3) (2021) 2089–2097.
 36. S. H. Mikaei *et al.*, Stability and anti-chaos control of discrete quadratic maps, *Iraqi J. Sci.* **62**(5) (2021) 1675–1685.
 37. F. Yuan, C.-J. Bai and Y.-X. Li, Cascade discrete memristive maps for enhancing chaos, *Chin. Phys. B* **30**(12) (2021) 120514–120514.
 38. B. Bao *et al.*, Memristor-coupled logistic hyperchaotic map, *IEEE Trans. Circuits Syst. II, Express Briefs* **68**(8) (2021) 2992–2996.
 39. L.-P. Zhang *et al.*, A novel class of two-dimensional chaotic maps with infinitely many coexisting attractors, *Chin. Phys. B* **29**(6) (2020) 060501.